UMSHA Press

AJEHE
Avicenna Journal of Environmental Health Engineering

Avicenna J Environ Health Eng. 2025;12(2):89-96. doi:10.34172/ajehe.5548

http://ajehe.umsha.ac.ir

Original Article

Photocatalysis-Adsorption of Amoxicillin from Water Using MgO-Biosilica Nanostructure

Reza Darvishi Cheshmeh Soltani[1], Mahdi Safari[2,3*], Reza Rezaee[2], Afshin Maleki[2], Behzad Shahmoradi[2]

[1]Department of Environmental Health, School of Health, Arak University of Medical Sciences, Arak, Iran
[2]Environmental Health Research Center, Research Institute for Health Development, Kurdistan University of Medical Sciences, Sanandaj, Iran
[3]Department of Environmental Health Engineering, Faculty of Health, Kurdistan University of Medical Sciences, Sanandaj, Iran

Article history:
Received: September 9, 2024
Revised: March 3, 2025
Accepted: August 28, 2025
ePublished: December 30, 2025

***Corresponding author:**
Mahdi Safari,
Email: Safari.m.eng@gmail.com

Abstract

The main objective of the present research study was the application of magnesium oxide (MgO) nanoparticles implanted in the matrix of biosilica for treating amoxicillin (AMX)-containing synthetic wastewater. Field emission scanning electron microscopy (FE-SEM) and X-ray diffraction (XRD) were used for the characterization. Although the efficiency of UV light alone was insignificant to degrade AMX (efficiency of 32%), the efficiency of the adsorption process was 42.6%, which implies the major role of the adsorption of AMX during its decomposition by photocatalysis. Regarding photocatalysis using MgO-implanted biosilica, increasing the initial pH from acidic to neutral conditions resulted in the enhanced removal of AMX (efficiency of 76%). At an optimum reaction time of 60 minutes and a photocatalyst dosage of 2 g/L, the removal efficiency (%) of AMX was found to be 94.9%. In the presence of 1 mM oxalic acid, the removal efficiency of AMX was 54.9%. The intermediate byproducts of AMX decomposition were also identified utilizing gas chromatography-mass spectroscopy (GC-MS) analysis. According to the results obtained, the treatment process of adsorption-photocatalysis using MgO-implanted biosilica can be recommended as an efficient technique for the degradation of pharmaceutical compounds such as AMX in aqueous environments.

Keywords: Advanced oxidation processes (AOPs), Photocatalyst, Nanostructured magnesium oxide, Pharmaceutical compounds, Immobilization

Please cite this article as follows: Darvishi Cheshmeh Soltani R, Safari M, Rezaee R, Maleki A, Shahmoradi B. Photocatalysis-adsorption of amoxicillin from water using MgO-biosilica nanostructure. Avicenna J Environ Health Eng. 2025;12(2):89-96. doi:10.34172/ajehe.5548

1. Introduction

The presence of pharmaceutically active compounds (PhACs) in aquatic environments has been identified as an emerging concern. Among various PhACs, antibiotic compounds have received specific consideration due to their acute and chronic adverse effects on human health as well as increasing bacterial resistance in aquatic ecosystems (1-3). Moreover, PhACs can cause adverse effects on terrestrial and aquatic life even at low concentrations (4). In Iran, more attention should be paid to the elimination of amoxicillin (AMX) due to its high consumption. More than 80% of AMX is not metabolized by the human body (3,5,6). Therefore, it is principally released into the aqueous environment through excretion, urine, and disposal of expired AMX capsules (7). Wastewater treatment systems cannot remove and degrade AMX molecules, resulting in the contamination of aquatic environments (4,8). Various treatment technologies are proposed to degrade and remove AMX. However, advanced oxidation processes (AOPs), including ozonation, Fenton, and photo-Fenton, are studied as the most effective treatment methods based on the generation of hydroxyl radicals ($OH^{\bullet}$) for the degradation of emerging refractory organic compounds such as pharmaceuticals (2,5,9). The photocatalytic process is one of the distinctive AOPs based on the generation of pair electron/hole on the surface of semiconductors and the subsequent generation of $OH^{\bullet}$ in the solution by the reaction of photo-generated holes (h^{+}) with water molecules (3,10,11). Many semiconductors are manufactured as photocatalysts to degrade target pollutants in the aqueous phase, including ZnO (12), TiO_2 (7,13), $BiPO_4$ (14), CdS (15), SnO_2 (16), HgS (17), Ag_3PO_4 (18), Ga_2O_3 (19), ZnS (20), ZrO_2 (21), CeO_2 (22), $BiVO_4$ (23), WO_3 (24), and so on. However, the development and application of magnesium oxide (MgO) as an efficient and novel catalyst draws more attention among researchers due to its non-toxic nature, excellent thermal and mechanical durability, large band

© 2025 The Author(s); Published by Hamadan University of Medical Sciences. This is an open-access article distributed under the terms of the Creative Commons Attribution License (https://creativecommons.org/licenses/by/4.0), which permits unrestricted use, distribution, and reproduction in any medium, provided the original work is properly cited.

gap, and low dielectric constant (25). The formation of $OH^{\bullet}$ during the photocatalysis using MgO nanoparticles is represented as follows:

$$MgO + h\nu \rightarrow MgO\left(e^{-} + h^{+}\right) \quad (1)$$

$$h^{+} + H_2O \rightarrow H^{+} + OH^{\bullet} \quad (2)$$

In our previous study, the sonocatalytic activity of MgO nanostructures was evaluated and proven to treat synthetic and real textile wastewaters (26). In the present study, apart from the application of MgO as a photocatalyst to decompose AMX, as-synthesized MgO nanoparticles were implanted in biosilica matrix to gain the advantages of immobilization. There was a successful experience regarding the application of biosilica as a support to immobilize ZnO nanoparticles in both sonocatalytic (27) and photocatalytic (12) reactors to treat textile wastewaters. The high porosity and consequently high surface area, along with a suitable solid matrix, make the biosilica a promising support to immobilize and implement nanostructured catalysts (12,27,28). Overall, the immobilization of nano-sized catalysts inhibits the release of nanoparticles into aqueous environments, improving cost-efficiency and the reusability potential of the catalyst (29). In addition, nanostructured photocatalysts are inclined to aggregate in the bulk solution, reducing their photocatalytic activity (7,30,31). However, the immobilization and implantation of nanostructures onto an appropriate carrier leads to the decomposition of fine particles in the solution (32). To the best of our knowledge, no research study has been conducted on the use of MgO-implanted biosilica for the photocatalytic degradation of AMX. In fact, MgO-implanted biosilica is not used as a photocatalyst for environmental remediation at all. The mineralization rate of the target pollutant and intermediate identification were considered. The antimicrobial activity of AMX-containing solutions was also investigated before and after photocatalysis by MgO-implanted biosilica under UV light irradiation.

2. Materials and Methods

2.1. Materials

Amoxicillin (molecular formula: $C_{16}H_{19}N_3O_5S$, molar mass: 365.4 g/mol, and CAS ID: 26787-78-0) and biosilica were purchased from Sigma-Aldrich, USA. Other materials and chemicals were obtained from Merck. $Mg(NO_3)_2{\cdot}6H_2O$ was used as the precursor of MgO nanoparticles. To synthesize and implant MgO nanoparticles, 5.128 g of $Mg(NO_3)_2{\cdot}6H_2O$ was dissolved in 100 mL of deionized water. Afterwards, 1 N NaOH solution was added slowly to the solution until its pH reached 10. The resulting suspension was magnetically stirred for 5 minutes. Then, 2.562 g of the biosilica was added to the resulting white precipitate and the mixture was kept under magnetic stirring for 10 minutes. The mixture was sonicated for 120 minutes at 50°C using an ultrasonic bath. In the following, the mixture was filtered and rinsed with deionized water and alcohol. Finally, the mixture was dried in an oven at 80 °C for 48 hours (33).

2.2. Experimental Set-up

A Plexiglas reactor with a working volume of 400 mL was applied to conduct the photocatalytic decomposition of AMX using MgO-implanted biosilica. Three 6-W low-pressure UVC lamps (lamp specification: wattage: 6W, amperage: 0.16A, voltage: 42V, spectral peak: 253.7 nm, length: 222.3 mm, diameter: 16 mm, Philips, the Netherlands) were used for irradiation. To keep the bulk solution homogeneous, it was stirred magnetically using a Heidolph magnetic shaker. To evaluate the effect of the adsorption process on the removal of AMX, the photoreactor was placed in the dark.

2.3. Analysis

A KNAUER high performance liquid chromatography (HPLC, Model: AZURA, Germany) was used to measure the concentration of AMX in as-prepared samples. The instrument was equipped with a NUCLEODUR 100-5 C18 column (25 cm × 4.6 mm × 5 u) and a UV detector (working wavelength of 254 nm) operated at room temperature. The mobile phase consisted of a mixture of phosphate buffer (pH: 4.5) and methanol with the volumetric ratio of 60:40 (at a specified flow rate of 1 mL/min). Field emission scanning electron microscopy (FE-SEM) was used to evaluate particle size and surficial morphology of as-synthesized samples (TESCAN, Model: Mira3, Czech Republic). X-ray diffraction (XRD) was conducted using Cu as an anode material (PANalytical, Model: X'Pert Pro MPD, the Netherlands) to assess the crystallinity of the photocatalyst.

3. Results and Discussion

3.1. Morphological Investigation

FE-SEM images of pure MgO nanostructures and MgO-implanted biosilica are provided in Fig. 1. Fig. 1a displays that as-synthesized MgO structures are within the nano-range (lower than 100 nm). Fig. 1b indicates that the implantation of MgO nanoparticles in biosilica was carried out successfully. In fact, the porous structure of biosilica, which can be regularly seen in Fig. 1b, is an exceptional structure for the immobilization of nanostructured materials such as MgO. Fig. 2 exhibits the XRD pattern of MgO-implanted biosilica. As depicted, both MgO and biosilica peaks can be clearly observed. The peaks located at 21.81 and 26.72° are associated with biosilica structure according to JCPDS card number 00-001-0647 (12). The XRD pattern of MgO presented 4 diffraction peaks placed at 37.02°, 43.00°, 62.37°, and 74.64°, which are attributed to JCPDS card number 87-0653 (34).

3.2. Effect of Operational Parameters

The effect of operational conditions on the efficiency

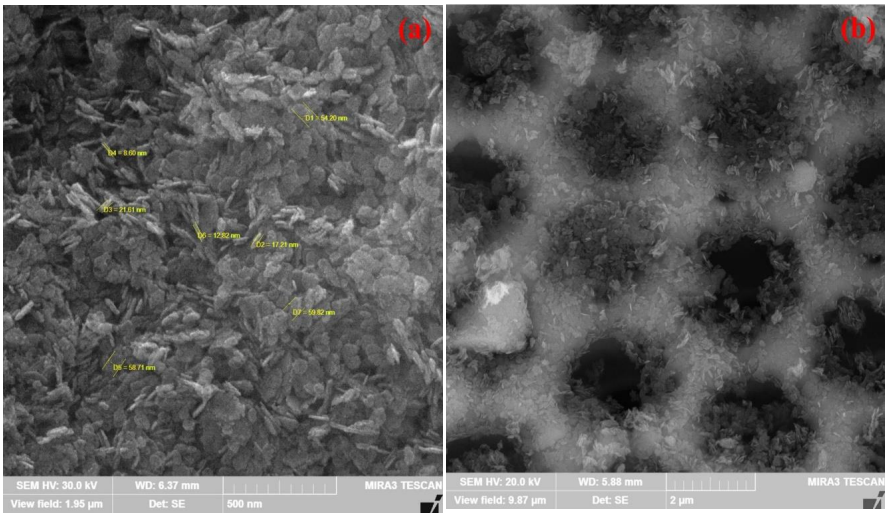

Fig. 1. FE-SEM Images of MgO Nanostructures (a) and MgO-implanted Biosilica (b)

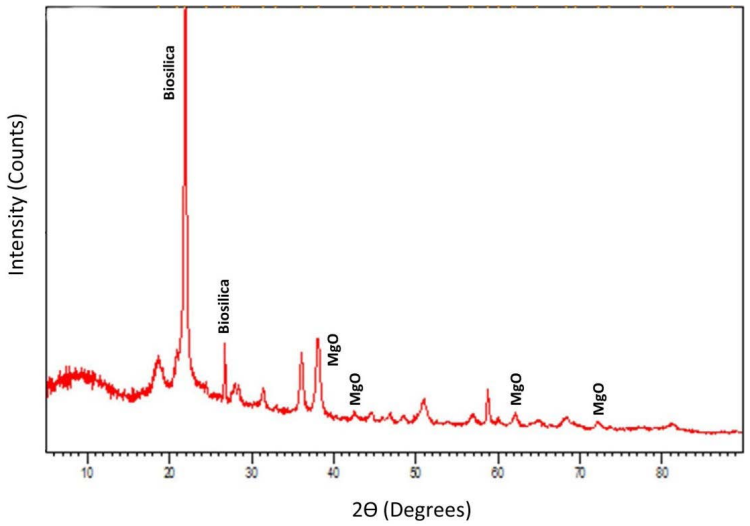

Fig. 2. XRD Pattern of MgO-Implanted Biosilica

of the treatment process was assessed using 4 main operational parameters, including initial pH, reaction time, MgO/biosilica dosage, and AMX concentration. In the following, the effect of the presence of competing organic compounds such as ethanol, methanol, oxalic acid, citric acid, EDTA, and phenol was also investigated. Before this, the role of each process involved in the removal of AMX via photocatalysis using MgO-implanted biosilica was specified under the same operational conditions (initial pH of 7, reaction time of 60 minutes, MgO/biosilica dosage of 1 g/L, and AMX concentration of 10 mg/L). According to the results, the efficiency of UV light alone was insignificant in the degradation of AMX (removal efficiency of 32%). The adsorption efficiency of AMX onto MgO-implanted biosilica was about 42.6%, indicating that the adsorption of AMX by the nanocomposite catalyst can be proposed as one of the main steps during the photocatalysis of AMX. In fact, the target pollutant is adsorbed onto the nanocomposite catalyst and then degraded through the hydroxyl radicals generated on the surface of the catalyst irradiated by UV light. The results demonstrated that the efficiency of the photocatalytic processes onto both MgO alone and MgO-implanted biosilica was very significant in comparison with the UV light alone (photolysis) and adsorption process. The efficiency of the MgO/UV process in the decomposition of AMX was 71.7%, while the efficiency of the photocatalysis using MgO-implanted biosilica (MgO/biosilica/UV) was 80.9% at a reaction time of 1 hour. This finding confirmed the fact that the immobilization of fine-sized catalyst onto a suitable support result in the de-aggregation of fine particles and higher photocatalytic activity for the degradation of the target pharmaceutical compound (32). The synergy percentage (%) of the MgO/biosilica/UV process in comparison with UV alone and adsorption alone was calculated by the following equation:

$$Synergy\ of MgO/biosilica/UV\,(\%) = \frac{RE_{MgO/biosilica/UV} - \left(RE_{MgO/biosilica} + RE_{UV}\right)}{RE_{MgO/biosilica/UV}} \times 100 \quad (3)$$

According to the above equation, the synergy percentage (%) was calculated to be 7.79%, implying the synergetic degradation of AMX by the MgO/biosilica/UV process in comparison with the individual processes of adsorption and photolysis (UV alone).

3.2.1. Initial pH

The initial pH of the bulk solution plays an important role in the photocatalysis of the target pollutant due to its effect on the generation of free radical species and the surface characteristics of the catalyst. In this regard, the initial pH of the reactor varied from 3 to 11, while the reaction time, MgO/biosilica dosage, and AMX concentration were fixed at 60 minutes, 1 g/L, and 10 mg/L, respectively. The results presented in Fig. 3 shows that increasing pH from acidic to neutral conditions results in an enhanced removal of AMX (up to 76%), while increasing pH from neutral to alkaline conditions resulted in an insignificant increase in the removal efficiency (82.9% at a pH value of 11).

Overall, increasing the initial pH favored the degradation of AMX by the photocatalysis using MgO-implanted biosilica. To interpret these results, the zero-point charge (pHzpc) of the nanocomposite catalyst was determined. The immobilized MgO pHzpc of around 12 indicated that the surface charge of the catalyst was positive at pH values below 12. Therefore, the surface charge of the catalyst is positive throughout the ranges of pH studied. In the case of AMX, it varies from positive in acidic conditions to negative charge in basic conditions (35). Under acidic conditions, both catalyst and AMX are positively charged; therefore, the adsorption of AMX onto the catalyst and subsequent degradation were limited. Under basic conditions, the adsorption of negatively charged AMX onto the surface of the positively charged catalyst is desirable for efficient adsorption. Moreover, increasing the removal efficiency of AMX at basic conditions can be attributed to the presence of large amounts of hydroxyl ions (OH^-), favoring the generation of hydroxyl radicals ($OH^{\bullet}$) on the surface of the catalyst (10). Considering both application viewpoint and economic aspects, the neutral pH of 7 was chosen as the optimal value for performing the rest of the experiments. Seid-Mohammadi et al showed that by reducing the initial pH from 11 to 3, the pollutant removal efficiency increased from 66% to 95%. They reported that MgO in acidic conditions can generate more hydroxyl radicals, which have the highest redox potential (28).

3.2.2. Reaction Time

The reaction time for the decomposition of AMX through the photocatalysis ranged between 10 and 180 minutes. Fig. 4 indicates the obtained results. As can be observed from the time profile, the adsorption and subsequent photocatalysis of AMX were fast at the beginning of the process, but the rate of adsorption gradually slowed down as the reaction time was extended until reaching equilibrium. As depicted, the removal efficiency (%) of AMX sharply increased from 40.4 to 80.9% with an increase in the time from 10 to 60 minutes, respectively. However, increasing the time from 60 to 180 minutes led to an insignificant increase in efficiency. In this period of time, the efficiency of removal increased by 10%. This trend, which was observed in the present study, may be ascribed to the large number of unoccupied active sites available for the adsorption and subsequent degradation of AMX molecules at the initial stages of the process (36). A similar trend was observed by Shi et al in their study on the photocatalysis of a pharmaceutical compound using Cu_2O–TiO_2 composite photocatalyst (7). Next, the reactor was operated with a reaction time of 60 minutes to conduct the following experiments, considering the cost-effectiveness of the process.

3.2.3. MgO/Biosilica Dosage

The photocatalytic process of AMX depends on the dosage of MgO-implanted biosilica as a nanocomposite photocatalyst. For this purpose, the catalyst dosage was changed within the range of 0.3-2 mg/L. Fig. 5 shows that increasing the dosage from 0.3 to 2 g/L resulted in an increase in the removal efficiency (%) of AMX from 34.2 to 94.9%, respectively. Therefore, increasing the dosage of MgO-implanted biosilica favors the photocatalysis of AMX. Therefore, increasing the dosage of the

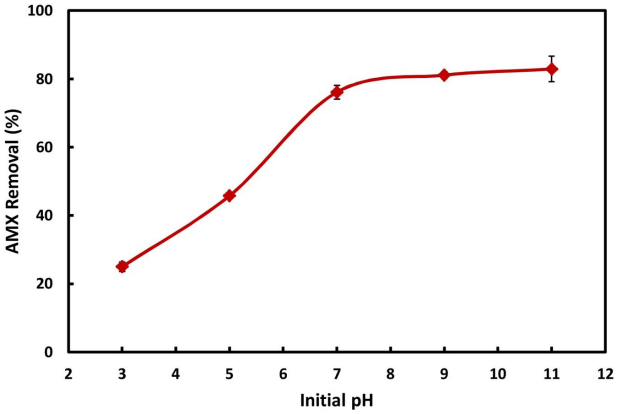

Fig. 3. Effect of Initial pH on the Removal of AMX via Photocatalysis

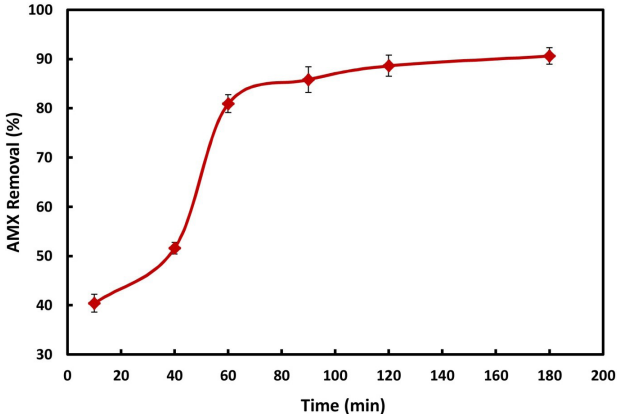

Fig. 4. Effect of Reaction Time on the Efficiency of the Photocatalytic Process

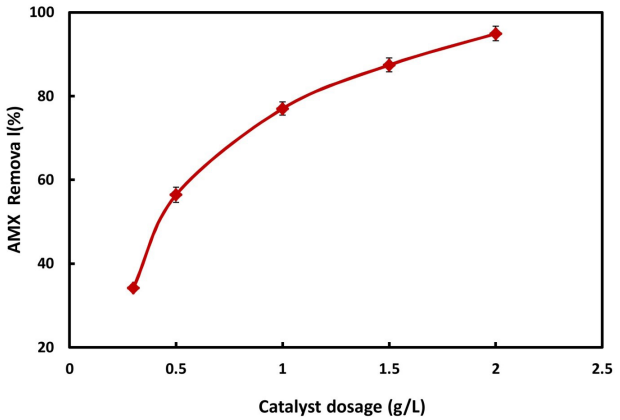

Fig. 5. Effect of Photocatalyst Dosage on the Removal Efficiency (%) of AMX

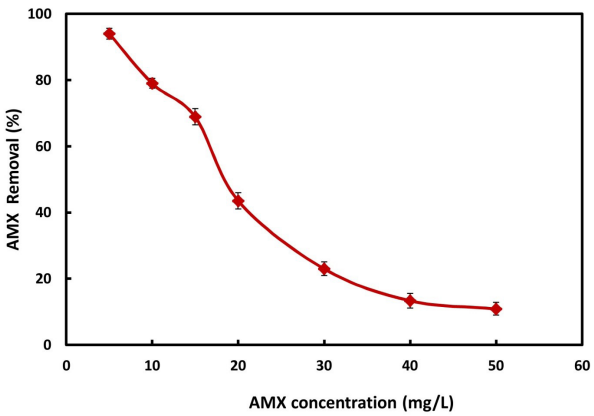

Fig. 6. Effect of AMX Concentration on its Removal Efficiency

nanocomposite catalyst provides higher active sites for the adsorption and decomposition of AMX.

The higher the dosage of photocatalyst, the greater the availability of active surface sites (37). Moreover, the increased surface area is advantageous for UV light adsorption, leading to the enhancement of hydroxyl radical generation on the catalyst surface for the degradation of the target pharmaceutical pollutant (12,34). On the other hand, the efficiency of UV light adsorption is enhanced with increasing the dosage of the applied photocatalyst (30). Qu et al reported similar results in the case of the photocatalytic degradation of an antibiotic drug using TiO_2/grapheme/activated carbon nanocomposite (38). Enhanced photocatalytic decomposition of AMX with increasing the dosage of catalyst indicated a heterogeneous photocatalytic regimen since the fraction of light absorbed by the catalyst gradually increased in the solution containing higher dosages of the catalyst (2). However, an optimum value of the applied catalyst should be selected to operate the process and improve its cost-efficiency. Elmolla and Chaudhuri reported that increasing the catalyst concentration from 0.5 to 1.0 g/L increased the degradation efficiency. However, increasing the catalyst concentration above 1 g/L did not significantly improve the degradation of the antibiotic. They stated that the high concentration of catalyst may reduce the penetration of light, resulting in more scattering of light, as well as accumulation and sedimentation of the catalyst (10).

3.2.4. Solute Concentration

It is essential to evaluate the effect of solute concentration (target pollutant concentration) on the efficiency of a treatment process. In the present study, the initial concentration of AMX was changed from 5 to 50 mg/L to assess the ability of MgO-implanted biosilica as a photocatalyst for the degradation of different concentrations of AMX under UV light irradiation. The results are shown in Fig. 6. Therefore, increasing the initial concentration of AMX caused a significant decrease in the efficiency of the treatment process. The removal efficiency (%) of AMX was obtained to be 94.0%, 79.0%, 68.9%, 43.5%, 23.0%, 13.3%, and 10.9% at concentrations of 5, 10, 15, 20, 30, 40, and 50 mg/L, respectively. The excessive concentrations of AMX may prevent the penetration of UV light into the catalyst efficiently generating hydroxyl radicals (39).

3.2.5. Presence of Competing Organic Compounds

To investigate the efficiency of the photocatalytic process under real conditions, its efficiency was checked in the presence of some prevalent competing organic compounds. For this purpose, the efficiency of the process was determined in the presence of ethanol, oxalic acid, methanol, EDTA, citric acid, and phenol at a concentration of 1 mM. Fig. 7 exhibits that the presence of all competing organic compounds leads to a decrease in the removal efficiency (%) of AMX. However, the inhibitory effect of oxalic acid, EDTA, and citric acid was dominant. Compared with the efficiency of the control reactor without competing organic compounds (78.3%), the efficiency of the process in the presence of ethanol, oxalic acid, methanol, EDTA, citric acid, and phenol was found to be 69.2%, 54.9%, 66.8%, 57.5%, 59.3%, and 66.3%, respectively. The decrease in the AMX removal in the presence of some competing organic compounds with radical scavenging properties indirectly demonstrated the fundamental role of photo-catalytically generated $OH^{\bullet}$ in the degradation of the target pollutant.

3.3. Detection of Byproducts

The results of GC-MS analysis, which are provided in Table 1, were employed in order to show intermediate byproducts generated during the photocatalysis of AMX. The formation of intermediate byproducts with lower molecular weights indicated the good progress in the degradation of AMX by photocatalysis using MgO-implanted biosilica. However, the reaction time (60 minutes) applied for the photocatalysis of AMX was not sufficient to decompose the parent compound into inorganic byproducts.

4. Conclusion

The photocatalytic process using MgO-implanted biosilica was employed to decompose AMX in the aquatic

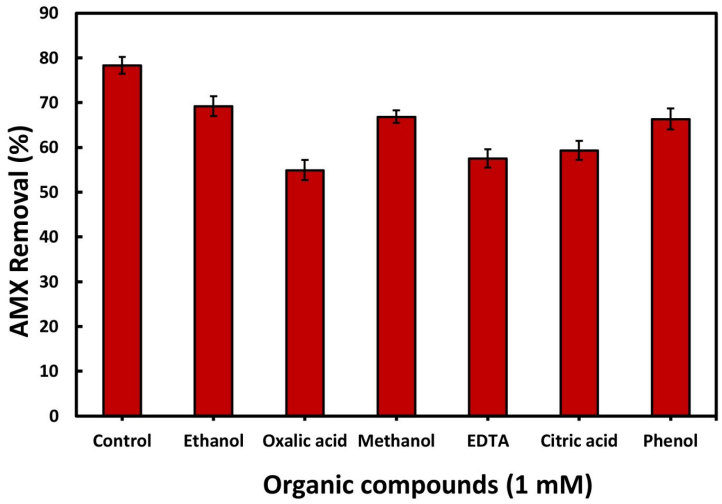

Fig. 7. Effect of Organic Competing Compounds on the Decomposition of AMX by Photocatalysis Using MgO-implanted Biosilica in Comparison with the Control Sample

Table 1. Identified Intermediates Generated during the Photocatalytic Degradation of AMX by MgO Nanoparticles-implanted Biosilica

No.	Compound	Molecular formula	Molecular weight (g/mole)	Retention time (min)
1	Amoxicillin	$C_{16}H_{19}N_3O_5S$	365.4	0.00
2	p-Menth-1-en-3-one, semicarbazone	$C_{11}H_{19}N_3O$	209.29	8.849
3	cis-4-Ethoxy-b-methyl-b-nitrostyrene	$C_{11}H_{13}NO_3$	207.23	6.257
4	4-(4-Methoxyphenoxy)-1,2,5-oxadiazol-3-amine	$C_9H_9N_3O_3$	207.19	6.474
5	Methyl 1-deoxy-6-thio-D-fructopyranoside	$C_7H_{14}O_4S$	194.25	11.269
6	Thiiranecarboxamide, 2-methyl-N-phenyl	$C_{10}H_{11}NOS$	193.27	12.728

phase. Scanning electron microscopy confirmed the good structure of MgO alone and its immobilized form covering the biosilica bio-structure. The XRD pattern of MgO-implanted biosilica was also used to demonstrate the suitable structure of the nanocomposite catalyst for the photocatalysis of AMX in the solution. Preliminary results revealed that the adsorption of AMX onto the nanocomposite catalyst can play a major role in its removal from the bulk solution. Results indicated that the treatment process was pH dependent and was also influenced by the initial AMX concentration and catalyst dosage. Most of the AMX molecules were decomposed in a short period of time. The efficiency of the process was adversely affected in the presence of competing organic compounds, especially oxalic acid, EDTA, and citric acid. The identified intermediate byproducts generated during the photocatalysis of AMX indicated the need for longer exposure time for the complete decomposition of the parent compound. Overall, it can be concluded that the photocatalytic process of MgO/bioslica/UV can be applied as an effective treatment process to decontaminate AMX-containing water and wastewater.

Acknowledgements
The authors would like to thank Kurdistan University of Medical Sciences, Sanandaj, Iran, for providing financial and instrumental support.

Authors' Contribution
Conceptualization: Mahdi safari, Reza rezaee.
Methodology: Reza Darvishi cheshmeh soltani, Mahdi safari.
Project administration: Mahdi safari.
Writing – original draft: Reza Darvishi cheshmeh soltani, Behzad Shahmoradi.
Writing – review & editing: Mahdi safari, Afshin Maleki.

Competing Interests
None.

Ethical Approval
The protocol and procedures of this study were approved by the Ethics Committee of Kurdistan University of Medical Sciences (IR.MUK.REC.1395/325).

Funding
This study was funded by Kurdistan University of Medical Sciences 19178.

References
1. Gozlan I, Rotstein A, Avisar D. Amoxicillin-degradation products formed under controlled environmental conditions: identification and determination in the aquatic environment. Chemosphere. 2013;91(7):985-92. doi: 10.1016/j.chemosphere.2013.01.095.
2. Dimitrakopoulou D, Rethemiotaki I, Frontistis Z, Xekoukoulotakis NP, Venieri D, Mantzavinos D. Degradation, mineralization and antibiotic inactivation of amoxicillin by UV-A/TiO_2 photocatalysis. J Environ Manage. 2012;98:168-74. doi: 10.1016/j.jenvman.2012.01.010.
3. Calcio Gaudino E, Canova E, Liu P, Wu Z, Cravotto G. Degradation of antibiotics in wastewater: new advances in cavitational treatments. Molecules. 2021;26(3):617. doi: 10.3390/molecules26030617.
4. Souza FS, da Silva VV, Rosin CK, Hainzenreder L, Arenzon A, Féris LA. Comparison of different advanced oxidation processes for the removal of amoxicillin in aqueous

solution. Environ Technol. 2018;39(5):549-57. doi: 10.1080/09593330.2017.1306116.
5. Pereira JH, Reis AC, Nunes OC, Borges MT, Vilar VJ, Boaventura RA. Assessment of solar driven TiO2-assisted photocatalysis efficiency on amoxicillin degradation. Environ Sci Pollut Res Int. 2014;21(2):1292-303. doi: 10.1007/s11356-013-2014-1.
6. Homem V, Alves A, Santos L. Amoxicillin removal from aqueous matrices by sorption with almond shell ashes. Int J Environ Anal Chem. 2010;90(14-15):1063-84. doi: 10.1080/03067310903410964.
7. Shi Y, Yang Z, Wang B, An H, Chen Z, Cui H. Adsorption and photocatalytic degradation of tetracycline hydrochloride using a palygorskite-supported Cu2O–TiO2 composite. Appl Clay Sci. 2016;119(Pt 2):311-20. doi: 10.1016/j.clay.2015.10.033.
8. Elhaci A, Labed F, Khenifi A, Bouberka Z, Kameche M, Benabbou K. MgAl-Layered double hydroxide for amoxicillin removal from aqueous media. Int J Environ Anal Chem. 2021;101(15):2876-98. doi: 10.1080/03067319.2020.1715374.
9. Jung YJ, Kim WG, Yoon Y, Kang JW, Hong YM, Kim HW. Removal of amoxicillin by UV and UV/H2O2 processes. Sci Total Environ. 2012;420:160-7. doi: 10.1016/j.scitotenv.2011.12.011.
10. Elmolla ES, Chaudhuri M. Degradation of amoxicillin, ampicillin and cloxacillin antibiotics in aqueous solution by the UV/ZnO photocatalytic process. J Hazard Mater. 2010;173(1-3):445-9. doi: 10.1016/j.jhazmat.2009.08.104.
11. Samarghandi MR, Rahmani AR, Samadi MT, Kiamanesh M, Azarian G. Degradation of pentachlorophenol in aqueous solution by the UV/ZrO2/H2O2 photocatalytic process. Avicenna J Environ Health Eng. 2015;2(2):4761. doi: 10.17795/ajehe-4761.
12. Darvishi Cheshmeh Soltani R, Khataee AR, Mashayekhi M. Photocatalytic degradation of a textile dye in aqueous phase over ZnO nanoparticles embedded in biosilica nanobiostructure. Desalin Water Treat. 2016;57(29):13494-504. doi: 10.1080/19443994.2015.1058193.
13. Khataee AR, Kasiri MB. Photocatalytic degradation of organic dyes in the presence of nanostructured titanium dioxide: influence of the chemical structure of dyes. J Mol Catal A Chem. 2010;328(1-2):8-26. doi: 10.1016/j.molcata.2010.05.023.
14. Zhang Y, Selvaraj R, Sillanpää M, Kim Y, Tai CW. The influence of operating parameters on heterogeneous photocatalytic mineralization of phenol over BiPO4. Chem Eng J. 2014;245:117-23. doi: 10.1016/j.cej.2014.02.028.
15. Repo E, Rengaraj S, Pulkka S, Castangnoli E, Suihkonen S, Sopanen M, et al. Photocatalytic degradation of dyes by CdS microspheres under near UV and blue LED radiation. Sep Purif Technol. 2013;120:206-14. doi: 10.1016/j.seppur.2013.10.008.
16. Mohammed PS, Seyyedi K. Photocatalytic degradation of cefixime antibiotic by polyaniline/SnO2 nanocomposite and optimization of the process using response surface methodology. J Adv Environ Health Res. 2023;11(2):94-105. doi: 10.34172/jaehr.2023.12.
17. Selvaraj R, Qi K, Al-Kindy SM, Sillanpää M, Kim Y, Tai CW. A simple hydrothermal route for the preparation of HgS nanoparticles and their photocatalytic activities. RSC Adv. 2014;4(30):15371-6. doi: 10.1039/c4ra00483c.
18. Xiang Q, Lang D, Shen T, Liu F. Graphene-modified nanosized Ag3PO4 photocatalysts for enhanced visible-light photocatalytic activity and stability. Appl Catal B Environ. 2015;162:196-203. doi: 10.1016/j.apcatb.2014.06.051.
19. Lopes da Silva F, Laitinen T, Pirilä M, Keiski RL, Ojala S. Photocatalytic degradation of perfluorooctanoic acid (PFOA) from wastewaters by TiO2, In2O3 and Ga2O3 catalysts. Top Catal. 2017;60(17):1345-58. doi: 10.1007/s11244-017-0819-8.
20. Hanifehpour Y, Soltani B, Amani-Ghadim AR, Hedayati B, Khomami B, Joo SW. Praseodymium-doped ZnS nanomaterials: hydrothermal synthesis and characterization with enhanced visible light photocatalytic activity. J Ind Eng Chem. 2016;34:41-50. doi: 10.1016/j.jiec.2015.10.032.
21. Moradi M, Ghanbari F, Manshouri M, Angali KA. Photocatalytic degradation of azo dye using nano-ZrO2/UV/persulfate: response surface modeling and optimization. Korean J Chem Eng. 2016;33(2):539-46. doi: 10.1007/s11814-015-0160-5.
22. Ji P, Zhang J, Chen F, Anpo M. Ordered mesoporous CeO2 synthesized by nanocasting from cubic Ia3d mesoporous MCM-48 silica: formation, characterization and photocatalytic activity. J Phys Chem C. 2008;112(46):17809-13. doi: 10.1021/jp8054087.
23. Soma K, Iwase A, Kudo A. Enhanced activity of BiVO4 powdered photocatalyst under visible light irradiation by preparing microwave-assisted aqueous solution methods. Catal Lett. 2014;144(11):1962-7. doi: 10.1007/s10562-014-1361-y.
24. Shafaei N, Jahanshahi M, Peyravi M, Najafpour Q. Self-cleaning behavior of nanocomposite membrane induced by photocatalytic WO3 nanoparticles for landfill leachate treatment. Korean J Chem Eng. 2016;33(10):2968-81. doi: 10.1007/s11814-016-0154-y.
25. Darvishi Cheshmeh Soltani R, Safari M, Rezaee R, Maleki A, Giahi O, Ghanbari R. Sonocatalytic degradation of humic substances from aquatic environments using MgO nanoparticles. Avicenna J Environm Health Eng. 2017;4(2):13-8. doi: 10.15171/ajehe.2017.03.
26. Darvishi Cheshmeh Soltani R, Safari M. Periodate-assisted pulsed sonocatalysis of real textile wastewater in the presence of MgO nanoparticles: response surface methodological optimization. Ultrason Sonochem. 2016;32:181-90. doi: 10.1016/j.ultsonch.2016.03.011.
27. Darvishi Cheshmeh Soltani R, Jorfi S, Ramezani H, Purfadakari S. Ultrasonically induced ZnO-biosilica nanocomposite for degradation of a textile dye in aqueous phase. Ultrason Sonochem. 2016;28:69-78. doi: 10.1016/j.ultsonch.2015.07.002.
28. Seid-Mohammadi A, Bahrami M, Omari S, Asadi F. Removal of cephalexin from aqueous solutions using magnesium oxide/granular activated carbon hybrid photocatalytic process. Avicenna J Environ Health Eng. 2019;6(1):24-32. doi: 10.34172/ajehe.2019.04.
29. Rezaee A, Masoumbeigi H, Darvishi Cheshmeh Soltani R, Khataee AR, Hashemiyan S. Photocatalytic decolorization of methylene blue using immobilized ZnO nanoparticles prepared by solution combustion method. Desalin Water Treat. 2012;44(1-3):174-9. doi: 10.1080/19443994.2012.691700.
30. Chen Y, Liu K. Preparation and characterization of nitrogen-doped TiO2/diatomite integrated photocatalytic pellet for the adsorption-degradation of tetracycline hydrochloride using visible light. Chem Eng J. 2016;302:682-96. doi: 10.1016/j.cej.2016.05.108.
31. Wang B, de Godoi FC, Sun Z, Zeng Q, Zheng S, Frost RL. Synthesis, characterization and activity of an immobilized photocatalyst: natural porous diatomite supported titania nanoparticles. J Colloid Interface Sci. 2015;438:204-11. doi: 10.1016/j.jcis.2014.09.064.
32. Darvishi Cheshmeh Soltani R, Rezaee A, Khataee A. Combination of carbon black–ZnO/UV process with an electrochemical process equipped with a carbon black–PTFE-coated gas-diffusion cathode for removal of a textile dye. Ind Eng Chem Res. 2013;52(39):14133-42. doi: 10.1021/ie402478p.
33. Anilkumar MR, Nagaswarupa HP, Nagabhushana H, Sharma SC, Vidya YS, Anantharaju KS, et al. Bio-inspired route for the synthesis of spherical shaped MgO:Fe(3+) nanoparticles:

Structural, photoluminescence and photocatalytic investigation. Spectrochim Acta A Mol Biomol Spectrosc. 2015;149:703-13. doi: 10.1016/j.saa.2015.05.003.
34. Jorfi S, Barzegar G, Ahmadi M, Darvishi Cheshmeh Soltani R, Jafarzadeh Haghighifard N, Takdastan A, et al. Enhanced coagulation-photocatalytic treatment of acid red 73 dye and real textile wastewater using UVA/synthesized MgO nanoparticles. J Environ Manage. 2016;177:111-8. doi: 10.1016/j.jenvman.2016.04.005.
35. Elmolla ES, Chaudhuri M. Photocatalytic degradation of amoxicillin, ampicillin and cloxacillin antibiotics in aqueous solution using UV/TiO2 and UV/H2O2/TiO2 photocatalysis. Desalination. 2010;252(1-3):46-52. doi: 10.1016/j.desal.2009.11.003.
36. Hassan AF, Elhadidy H, Abdel-Mohsen AM. Adsorption and photocatalytic detoxification of diazinon using iron and nanotitania modified activated carbons. J Taiwan Inst Chem Eng. 2017;75:299-306. doi: 10.1016/j.jtice.2017.03.026.
37. Martins AF, Mayer F, Confortin EC, Frank CD. A study of photocatalytic processes involving the degradation of the organic load and amoxicillin in hospital wastewater. Clean Soil Air Water. 2009;37(4-5):365-71. doi: 10.1002/clen.200800022.
38. Qu LL, Wang N, Li YY, Bao DD, Yang GH, Li HT. Novel titanium dioxide–graphene–activated carbon ternary nanocomposites with enhanced photocatalytic performance in rhodamine B and tetracycline hydrochloride degradation. J Mater Sci. 2017;52(13):8311-20. doi: 10.1007/s10853-017-1047-0.
39. Yener HB, Yılmaz M, Deliismail Ö, Özkan SF, Helvacı ŞŞ. Clinoptilolite supported rutile TiO2 composites: synthesis, characterization, and photocatalytic activity on the degradation of terephthalic acid. Sep Purif Technol. 2017;173:17-26. doi: 10.1016/j.seppur.2016.09.010.